Watt-level SHG in undoped high step-index PPLN ridge waveguides

VINCENT PECHEUR,[1], HENRI PORTE,[2], JÉRÔME HAUDEN[2],FLORENT BASSIGNOT[3],MOISE DEROH[1] AND MATHIEU CHAUVET[1*]

[1]*FEMTO-ST Institute, CNRS, University of Bourgogne Franche-Comté, 15B avenue des Montboucons, 25000 Besançon, France*
[2]*iXblue Photonics,3 Rue Sophie Germain, 25000 Besançon*
[3]*Femto-Engineering, 15B avenue des Montboucons, 25000 Besançon, France*
mathieu.chauvet@univ-fcomte.fr

Abstract: Nonlinear quadratic waveguides are key components to obtain efficient frequency conversion. The performances of highly multimode periodically poled lithium niobate (PPLN) ridge waveguides for high power CW SHG are presented. We report generation of 1 W of second harmonic on the fundamental guided mode with a conversion efficiency of 56% at telecom wavelengths. A stable nonlinear process is obtained despite use of an undoped congruent $LiNbO_3$ crystal. The input damage threshold of the ridge waveguide is found to set the maximum usable power.

1. Introduction

Optical frequency conversion is of interest for various domains such as astronomy where parametric upconversion from mid infrared to visible range is exploited for efficient detection [1, 2], for life science imaging and analysis of interfaces details [3,4] or for medical or safety applications based on spectroscopy in the terahertz range [5,6]. Quantum technologies have also strong interest in nonlinear optical materials especially for generation of entangled pairs of photons [7,8] and for cooling atoms [9–11]. The latter applications typically rely on CW watt level sources that take advantage of the mature technology of telecommunication components (tunable near infrared sources, modulators, optical amplifiers) in combination with efficient frequency conversion devices to shift the wavelength to the requested value by second harmonic generation (SHG).

Such SHG devices are often based on Lithium Niobate ($LiNbO_3$) crystals thanks to its high nonlinear second order coefficient, large transparency window and wavelength conversion versatility using the quasi-phase matching process. High power CW sources have been achieved in bulk periodically poled lithium niobate (PPLN) [12, 13] but it requires a high pump power with an optimized focusing in the PPLN crystal to reach fair conversion efficiency. Furthermore, these set-ups are too bulky for some applications. At the other end, nano-waveguides [14–16] and resonators [17] can reach very high conversion efficiencies but they operate at milliwatts power level due to the extreme light confinement that is prone to thermal or photorefractive (PR) instabilities. In addition, efficient light coupling in nano-waveguides is a hurdle to applications.

A compromise is found with PPLN waveguides of few tens of micrometers section. They indeed provide high conversion efficiency thanks to a confined interaction over several centimeters along with a straightforward coupling with single mode fiber (SMF). Several technologies are available to fabricate such waveguides. Zinc diffused [18], proton exchange [19] or Titanium diffused [20] waveguides provide a good control of the geometry but have a weak guidance. This weak guidance has drawbacks such as moderately confined modes, non optimal overlap between interacting modes and sensitivity to perturbation due to the PR effect [20].

Bonded waveguides are a good alternative since they offer an improved guidance and preserve the initial nonlinear properties of the bulk material. Such nonlinear structures consist in direct

bonding [15] or gluing [21] of LiNbO$_3$ to a substrate before shaping ridge waveguides by dicing [22, 23] or etching [15, 24]. Note that this fabrication technique suits to a variety of materials, either available as wafers or as small size crystals such as KTP [25]. For ridge PPLN waveguides, LiNbO$_3$ wafers doped with MgO or Zn [26, 27] are often used in order to reduce the PR effect. In addition, single mode or weakly multimode waveguides are often sought.

In the present work, SHG performances of highly multimode undoped PPLN ridge waveguides are instead used. We show that despite the highly multimode character and the absence of doping, the fabricated large step-index waveguides give a stable and high conversion efficiency with over 1 W of generated frequency-doubled telecom wavelengths on the fundamental mode. The influence of the PR effect is analyzed along with the maximum usable power.

2.   Design and Fabrication

The designed waveguide is intended for SHG of telecom wavelengths with high conversion efficiency. It is based on a type-0 configuration with both pump and SH modes extraordinary polarized to exploit the strongest nonlinear coefficient d$_{33}$ of LiNbO$_3$. The waveguide is constituted of a square LiNbO$_3$ core sitting on a silica layer. Such an arrangement gives a strong guiding effect which has several advantages. First, both pump and SH fundamental modes have very similar profiles thus maximizing the nonlinear conversion through an optimum overlap integral. More importantly, the guiding effect is unaffected by instabilities due to thermal or PR effects. While the large core-cladding index difference also offers the possibility of a beneficial strong confinement we instead favoured a larger core size with a square section of about 8 μm in order to have an efficient direct coupling with a SMF. Despite the multimode character of the waveguide the phase matching condition for the SHG process provides a nonlinear interaction between the sole fundamental modes of the pump and SH signal [28]. For a given pump wavelength and waveguide structure, the phase matching can be engineered by choosing the proper poling period Λ for the LiNbO$_3$ core :

$$\Lambda = \frac{\lambda_\omega}{2(n_{2\omega} - n_\omega)} \tag{1}$$

where n$_\omega$ and n$_{2\omega}$ are respectively the effective indices of the pump and SH signal fundamental modes. They are calculated with a commercial software (COMSOL). The refractive index of congruent undoped LiNbO3 is taken from [29].

The first part of our fabrication process [28] is the electric poling of a 500 μm thick undoped congruent z-cut LiNbO$_3$ wafer (figure 1.a). Poling periods between 17.4μm and and 18.2 μm are chosen to obtain phase matching for pump wavelengths spanning from 1535 nm to 1570 nm. Once the poling is realized, we deposit a 600 nm thick buffer layer of silica on one side of the LiNbO$_3$ wafer (figure 1.b), followed by the sputtering of 300 nm of gold (figure 1.c). A gold layer of similar thickness is then deposited on a 500 μm thick high flatness silicon wafer. The bonding of both wafers is realized with a wafer bonder. This pressure-induced bonding [30] is made at room temperature (figure 1.d) in order to prevent mechanical stress due to the different thermal expansion coefficients of silicon and LiNbO$_3$. The PPLN side of the structure is then ground and polished by mechanical process (figure 1.e) until we reach the desired thickness. The last step consists in dicing the waveguides (figure 1.f) with a precision saw equipped with a polishing diamond blade. Fabricated ridge waveguides have typical cross section of 8x8 μm^2 and a length of 2 cm.

Figure 2 shows a SEM image of a typical waveguide. Its cross section is close to the targeted square shape. The corners of the waveguide are sharp with no sign of cracks. Top surface roughness (1 nm RMS) given by the polishing process is slightly better than side faces (4 nm RMS) obtained by the polishing saw. The uniform Si/gold/silica/LiNbO$_3$ interface, also visible in Fig. 2, indicates a homogeneous bonding.
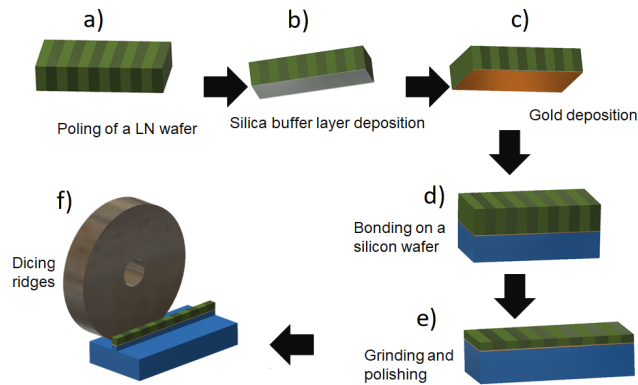
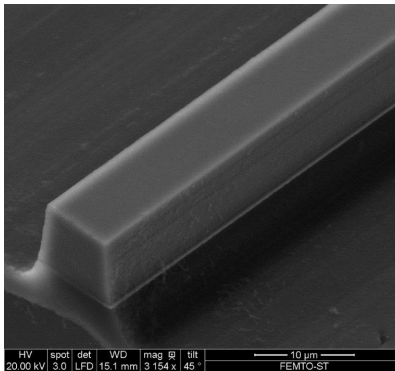Fig. 1. Description of each step of the fabrication of the ridge waveguides

Fig. 2. SEM image of a typical fabricated waveguide.

The waveguides are then tested to characterize their linear and nonlinear optical properties.

3. Optical characterization

To start, propagation losses are measured at 1.55 μm with a commercial equipment (LUNA obr4600). It is estimated to 0.6±0.2 dB/cm for TM polarization. In future developments a thicker silica buffer layer should lower propagation losses as expected from numerical simulations (not shown here).
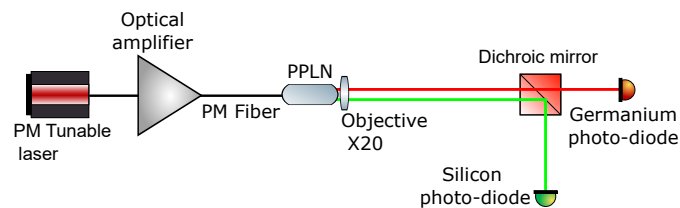

Fig. 3. Scheme of the experimental setup used for the optical characterization of the PPLN waveguides

Figure 3 shows a scheme of the setup used to characterize the PPLN waveguides. The optical source is a fibered linearly polarized tunable laser (TUNICS T100S-HP) at telecom wavelengths.

The laser signal, that can be amplified by a polarization maintaining (PM) erbium-doped fiber amplifier (EDFA, Keopsys CEFA-C-PB-HP-PM-37), is injected in the waveguide by butt-coupling with a cleaved PM single mode fiber. The fiber-waveguide coupling efficiency is about 77%. The polarization extinction ratio at the output of the fiber is about 20 dB. Both SHG signal and residual pump are collected by a x20 objective at the output of the PPLN waveguide and split by a dichroic mirror. The SHG signal and pump residue are detected by a silicon and a germanium photodiode, respectively. This configuration allows the calculation of the conversion efficiency of the SHG process. The temperature of the sample is controlled by a Peltier element in order to stabilize the spectral response and tune the phase-matching condition.
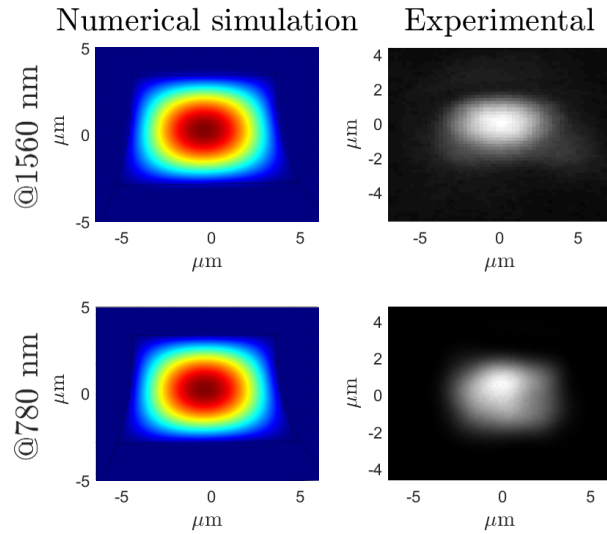

Fig. 4. Waveguide fundamental modes computed (left) and measured (right) for both the pump (top) and the signal (bottom) wavelengths

One necessity is to minimize the pump coupling to higher order guided modes and thus optimize the excitation of the fundamental mode since the most efficient interaction is between pump and SH fundamental modes. Note that the waveguide supports about 200 modes. The tested waveguide with a cross section of 7.1 μm high by 9.7 μm width has computed modes at $1/e^2$ of 5.2 by 7.7 μm^2 for the SH and 5.3 by 7.9 μm^2 for the pump as depicted in the left column in figure 4. As expected from a high step index waveguide, both fundamental modes are very close in size which provides a good overlap. Because of the multimode character of the waveguide, light coupling is a key point to obtain a maximum SHG conversion efficiency. It is performed by monitoring the SH signal level for the phase matched pump wavelength while adjusting the light coupling with a piezoelectric actuator. As observed at the output of the waveguide (figure 4 right column), the pump and the SH generated mode are indeed mostly propagating on the fundamental mode.

We then characterize the waveguide nonlinear properties at low pump power by scanning the pump wavelength in order to deduce the normalized conversion efficiency defined as $\eta = P_{2\omega}/P_\omega^2$ with $P_{2\omega}$ the SH output power and P_ω the pump input power.

Figure 5 shows the experimental and numerical simulation spectral responses of the waveguide in the undepleted pump regime. The maximum normalized conversion efficiency at 1562.3 nm is close to 88 %/W with presence of oscillations due to the Fabry-Pérot resonances between the two facets of the waveguide. The observed asymmetry of the experimental spectrum is due to variations of the waveguide cross section along propagation. It is mainly accountable for the
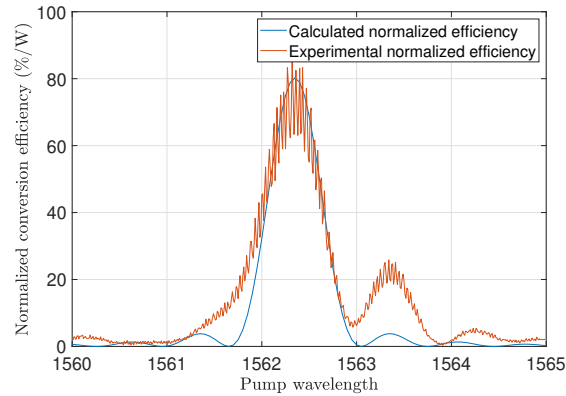
Fig. 5. Normalized conversion efficiency at 30°C of a 7.1 by 9.7 μm^2 cross section 2cm long PPLN waveguide with a poling period of 18.1 μm

thickness non uniformity of the LiNbO$_3$ layer given by the grinding and polishing fabrication process [15, 31]. We have measured a non-uniformity of 200 nm over the 2 cm length of the waveguide. The FWHM of the spectral response is 0.65 nm which is slightly degraded compared with a perfectly uniform 2 cm long waveguide as confirmed with the theoretical fit. A perfect waveguide would reach a conversion efficiency of about 150%/W.
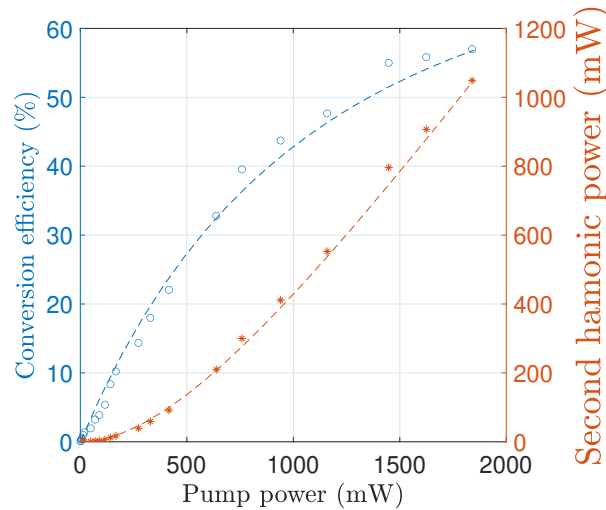

Fig. 6. SHG ouput power and efficiency conversion vs. injected pump power in the waveguide. Dots show the experimental data and the line curves show the numerical fits.

The component is then characterized at high power regime. Figure 6 depicts the conversion efficiency and SH signal power versus injected pump power measured for optimum phase-matching conditions in the previously described waveguide. For each measurement, we thus make sure the optimum pump wavelength and coupling condition are satisfied. The conversion efficiency is defined as $P_{2\omega}/P_\omega$. At low efficiency, under 10%, the SH power increases proportionally to the square of the pump power as expected from the undepleted pump model. The slope

confirms a normalized conversion efficiency of 88 %/W (22 %W^{-1}cm^{-2}). The pump power is then increased up to 1850 mW to generate 1040 mW of SH which corresponds to a conversion efficiency of 56%. We do not observe a power roll off as it is the case when parasitic effect strongly perturbs the phase matching condition, even though a slight influence of the PR effect is revealed later in the paper. Since conversion efficiency is no longer described by a analytic formula at high power we numerically solved the nonlinear coupled equations 2-3 [32] using a fourth order Runge-Kutta method. This model takes into account the depletion of the pump and includes the propagation losses in the waveguide.

$$\frac{dA_\omega}{dz} = \frac{2i\omega^2 d_{33}}{k_\omega c^2} A_{2\omega} A_\omega^* e^{-i\Delta kz} - \frac{\alpha}{2} A_\omega \tag{2}$$

$$\frac{dA_{2\omega}}{dz} = \frac{4i\omega^2 d_{33}}{k_{2\omega} c^2} A_\omega^2 e^{-i\Delta kz} - \frac{\alpha}{2} A_{2\omega} \tag{3}$$

where A_ω and $A_{2\omega}$ are the amplitude of the pump field and the SHG field along propagation in the crystal, respectively, $\Delta k = 2k_\omega - k_{2\omega}$ is the phase mismatch where k_ω is the pump propagation constant and $k_{2\omega}$ is the SH propagation constant and α is the propagation loss in the waveguide. α is set to 0.138 cm^{-1} in accordance with the above mentioned measured propagation losses. We consider the same propagation loss at both wavelengths since the measured total transmitted power does not depend on the phase matching condition even in the depleted pump regime. The poling of the crystal is taken into account by changing the sign of the nonlinear coefficient d$_{33}$ depending on the direction of the crystal c-axis.

As shown in Figure 6, this model give theoretical prediction in good agreement with the experimental data. It is important to note that it constitutes an additional hint that most of the light is indeed coupled mainly to the fundamental mode.

Spectral response of SH signal dependence versus pump power was also investigated. Fig.7 shows the normalized SH spectrum for three different pump power. The blue curve shows the SHG response at 80 μW SH output power, the red curve at 209 mW and the green curve at 1040 mW power. No sign of deterioration of the SH spectrum is present at high pump power. The rise of the lateral peak at high power is due the saturation of the efficiency for the main peak. We however observe a blue-shift of the response as the power is increased. A temperature raise of the sample induced by the strong pump could be invoked but it can be excluded since it is instead known to give a shift of the SH response toward longer wavelengths. Moreover, the temperature should increase gradually with power and consequently produce a progressive shift in wavelength which is not the case in the experiment. The absence of an overall heating of the waveguide is confirmed in the last part of the paper. Many signs indicate that the PR effect is the main reason for this behavior as discussed below.

In LiNbO$_3$, the PR effect [33] is known to be driven by the photovoltaic current. Due to this current, light-generated electrons move in the direction of the crystal c-axis. This cumulative displacement of charges leads to negative charges concentration on the Z+ side of the LiNbO$_3$ layer at the expense of positive charges on the other side. A static space charge field arises until it compensates the photovoltaic current. At equilibrium state the amplitude of this space charge field E$_{ph}$, which is oriented along the crystal c-axis and thus positive, can reach several kV/cm [33]. It decreases the refractive index through the Pockels effect which modifies in turn the phase-matching conditions. The shift in wavelength of the SHG response is given by the following equation: [20]:

$$\Delta\lambda_\omega = 2\Lambda(\Delta n_{2\omega} - \Delta n_\omega) \tag{4}$$

with Δn_{SH} and Δn_{pump} the mode effective index change for the SH and pump, respectively.

For the present configuration the change of refractive index by Pockels effect is given by:

$$\Delta n = -\frac{1}{2}n^3 r_{33} E_{ph} \tag{5}$$

Where r_{33} is the electro-optic coefficient. The positive value of E_{ph} involves a decrease of the refractive index which has a larger amplitude for $\Delta n_{2\omega}$ than for Δn_ω due to the refractive index dispersion. According to eq.4 a blue shift of the SHG response is thus expected as observed experimentally. Moreover, E_{ph} is known to saturate as the intensity is raised [20]. This nonlinear intensity behavior is present in Fig.7 where the steady-state shift of the SHG response is similar for a generated signal of 209 mW or 1040 mW. It is thus fair to assume that the photovoltaic field is already saturated with 209 mW of SH power. To the contrary, the SH response of the waveguide when SH power is more than three orders of magnitude lower (80 µW in Fig.7) corresponds to a situation with negligible PR effect. This spectral response was indeed consistently obtained when very low power SH signal was generated in waveguides that were previously left several hours resting. The shift of the phase-matching wavelength induced by the PR effect is thus evaluated to - 0.3 nm. Using equation 4, we can deduce that the amplitude of the PR field E_{ph} is about 0.9 kV.cm^{-1} which is consistent with values found in the literature [33] for undoped LiNbO$_3$. Note that our method is not adequate to precisely determine the response time of the PR effect since the characteristic time to acquire a spectrum with our computer controlled equipment is on the order of a minute. However, we observed that for a 200 mW generated SH a steady-state spectrum shift is attained after two successive spectrum acquisitions. With this procedure the PR establishment time is thus on the order of few minutes but it is expected to be much shorter if maximum conversion wavelength is kept instead of wavelength scanning. It is important to check that the PR effect build-up is negligible when an out of phase-matching 200 mW power pump is coupled in the waveguide. To do so, the first step consists in measuring the SHG response right after we turn on the laser. Then we let the sample rest for hours to be sure any PR field is erased. We raise the temperature of the sample to 55 °C, which is the highest temperature available on our setup, in order to erase the PR field faster. In a second step, we inject the same high power pump at a wavelength out of phase-matching for few tens of minutes before measuring the SHG response. We observe that both measured SHG responses are alike with unshifted SH response. It implies that infrared light has a negligible influence on the PR effect.

The PR effect is thus found to take place inside this undoped LiNbO$_3$ ridge waveguide under the influence of the generated SH signal. It induces a negative shift of the phase-matching wavelength but it does not preclude proper operation of the frequency conversion component at high power CW regime at near room temperature operation. The photo-induced PR index change only weakly affects the guidance of our high step-index waveguide contrary to dramatic perturbations observed in weakly guiding waveguides [20]. Evidently, the PR effect could be reduced by using magnesium doped LiNbO$_3$ [34] or by raising the components temperature [35] but the observed stable steady-state regime at high power let us foreseen viable applications even with undoped LiNbO$_3$ kept at room temperature.

Since no power roll off was noticed at high light fluence in the components (Figure 6), a study was conducted to determine the maximum power that the fabricated components can sustain. We found that the value is set by the input face damage threshold. Indeed, as the launched power reaches a particular threshold, a catastrophic damage of the input face of the waveguide occurs. As depicted in the SEM image in figure 8.a, the waveguide entrance is melted over few tens of micrometers and some droplets of LiNbO$_3$ have been ejected in the vicinity of the input waveguide. The damage power threshold has been evaluated using a systematic procedure on eight test waveguides. It consists in gradually increasing the injected pump until the waveguide transmission suddenly drops. The input facet melting is always at the origin of this light transmission degradation. These experiments give consistent value of the damage power threshold leading to a 2.5 W ±0.5 W (6 MW.cm^{-2}) maximum input power. The damage
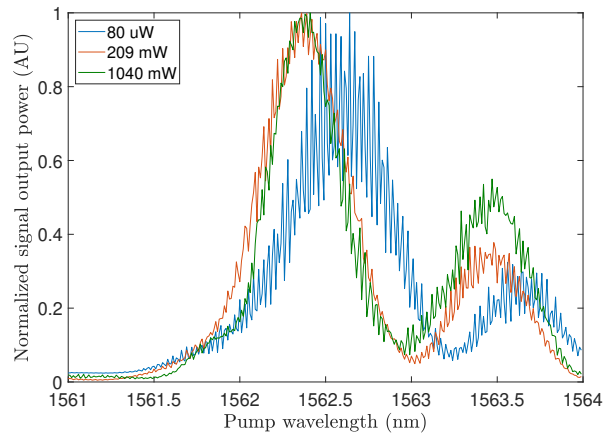
Fig. 7. Normalized SH spectrum response for 3 different output SH power at a temperature of 30°C.

threshold worsens when the fiber is not perfectly aligned with the waveguide. We also tested the influence of the smoothness of the input waveguide surface. The roughness (4-5 nm RMS) given by the dicing saw was improved using a local treatment with a focused ion beam instrument but it did not measurably increase the damage threshold power. The damage seems directly linked to the structure itself. An additional proof comes from the fact that bulk $LiNbO_3$ did not show any failure under twice the damage threshold intensity measured for waveguides. Note that a similar power limitation was also reported at telecom wavelengths in Zn-doped ridge waveguides [36]. They reported a 4.5 W damage threshold but for a wider incoming beam and in presence of antireflection coated surface. These results thus establish an upper limit of the usable CW power at telecom wavelengths in ridge PPLN waveguides. The observed local melting of the waveguide input led us to further analyse the temperature distribution of the waveguide under test. For this purpose an IR camera (FLIR A6700sc) and a CaF_2 lens are used to image the sample. A germanium filter is placed in front of the camera to remove any scattered light for the injected 1.55 μm pump. A thermal image of the previously characterized waveguide taken with this apparatus is shown in figure 8.b for a beam power of 0.8 W launched at the input facet of the waveguide sitting on a holder whose temperature is stabilized at 30°C. No significant temperature raise or gradient along the waveguide is observed. It confirms that the temperature increase of the waveguide is negligible and validates the above assumption that the PR effect is the dominant phenomena giving the shift of the SHG spectral response (Fig.7). However, a hot point is clearly seen in between the fiber and the input of the waveguide. This local hot point is undoubtedly the origin of the sample melting when the power damage threshold is exceeded. Note that the SMF is not damaged thanks to the small gap of air between the waveguide and the fiber and because of the different melting temperature of silica (1710°C) and $LiNbO_3$ (1257°C).

At last, we characterize the temperature tuning capabilities of our PPLN components. The main interest is obviously to finely adjust the operating point of the waveguide to a given phase matching wavelength but above all we have to verify the ability of our hetero-structures to sustain high temperature. The later concern arises from the very different thermal expansion coefficients of silicon ($2.6x10^{-6}$ K^{-1}) and $LiNbO_3$ ($15.4x10^{-6}$ K^{-1} along a-axis). For this purpose the sample holder is equipped with an oven in order to raise the PPLN sample. Figure 9 presents the measured central pump wavelength for a sample temperature varying from room temperature to 110°C. Some measured points are scattered due to a non optimized temperature regulation and also to the uncertainties to evaluate the central wavelength because of the Fabry-Pérot oscillations
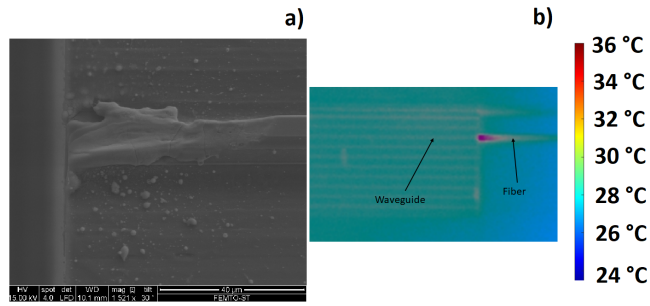
Fig. 8. SEM image of the input of a damaged waveguide (a). thermal image of the characterized waveguide thermalized at a temperature of about 30°C under test with a launched pump power of 0.8W (b)

in the spectral response (See Fig. 7). This temperature dependent study has been realized in the undepleted pump regime at mW pump level. Apart from the shift in wavelength no significant change of the conversion efficiency was observed.
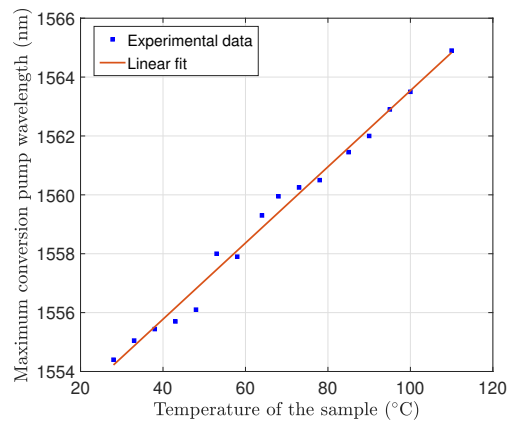

Fig. 9. Evolution of converted pump wavelength versus sample temperature.

A linear fit gives a slope of 0.132 nm°C^{-1} which is consistent with data obtained in bulk PPLN. No influence of strain is observed, More significantly the sample was even heated to 200°C and did not show any waveguide failure. .

4. Conclusion

We have shown that highly multimode ridge PPLN waveguides designed for SHG of telecom wavelengths give stable generation of over 1W output power in CW regime with an efficiency of 56%. The ridge waveguides are realized by mechanical thinning and precision dicing of a poled congruent undoped LiNbO$_3$ wafer bonded onto a silicon wafer. Experimental observations supported by modeling of the conversion efficiency with depleted pump corroborate that the SH signal is generated on the fundamental guided mode. At high power the component frequency conversion response is subject to a subnanometer blue-shift attributed to the PR effect present in the undoped LiNbO$_3$ active layer. A stable frequency conversion operation at large power is obtained thanks to the large index-step waveguiding structure. The maximum usable pump power near 2.5 W is set by the damage threshold of the input face of the waveguide. These nonlinear

chips constituted of a LiNbO$_3$/silicon heterostructure have been tested at temperature as high as 200°C which allow temperature tuning of the converted wavelength similarly than in bulk PPLN.

This work reveals that high step-index ridge waveguides made of undoped PPLN are suitable for efficient frequency conversion even when high power generation is requested such as laser cooling of atoms. We believe this configuration offers a viable alternative to singlemode or weakly multimode ridge waveguides based on doped LiNbO$_3$. Note that improved performances are attainable by simple technical steps such as a thicker SiO$_2$ buffer layer to lower losses and with anti-reflection coatings against parasitic Fabry-Pérot effects.

5. acknowledgment

6. Disclosures

The authors declare no conflicts of interest.

References

1. L. Lehmann, L. Grossard, L. Delage, F. Reynaud, M. Chauvet, F. Bassignot, F. Martinache, F. Morand, J.-P. Rivet, F.-X. Schmider, and D. Vernet, "Towards a mid-infrared l band up-conversion interferometer: first on-sky sensitivity test on a single arm," Mon. Notices Royal Astron. Soc. **485**, 3595–3599 (2019).
2. L. Lehmann, L. Grossard, L. Delage, F. Reynaud, M. Chauvet, and F. Bassignot, "Single photon MIR upconversion detector at room temperature with a PPLN ridge waveguide," Opt. Express **27**, 19233 (2019).
3. M. Han, G. Giese, and J. F. Bille, "Second harmonic generation imaging of collagen fibrils in cornea and sclera," Opt. Express **13**, 5791 (2005).
4. Y. R. Shen, "Surface properties probed by second-harmonic and sum-frequency generation," Nature **337**, 519–525 (1989).
5. W. Shi and Y. J. Ding, "Designs of terahertz waveguides for efficient parametric terahertz generation," Appl. Phys. Lett. **82**, 4435–4437 (2003).
6. Y.-S. Lee, T. Meade, T. B. Norris, and A. Galvanauskas, "Tunable narrow-band terahertz generation from periodically poled lithium niobate," in *Technical Digest. Summaries of papers presented at the Quantum Electronics and Laser Science Conference. Postconference Technical Digest (IEEE Cat. No.01CH37172),* (Opt. Soc. America, 2001).
7. D. Bouwmeester, J.-W. Pan, K. Mattle, M. Eibl, H. Weinfurter, and A. Zeilinger, "Experimental quantum teleportation," Nature **390**, 575–579 (1997).
8. S. Arahira, N. Namekata, T. Kishimoto, H. Yaegashi, and S. Inoue, "Generation of polarization entangled photon pairs at telecommunication wavelength using cascaded χˆ(2) processes in a periodically poled LiNbO_3 ridge waveguide," Opt. Express **19**, 16032 (2011).
9. A. Aspect, J. Dalibard, A. Heidmann, C. Salomon, and C. Cohen-Tannoudji, "Cooling atoms with stimulated emission," Phys. Rev. Lett. **57**, 1688–1691 (1986).
10. H. Metcalf and P. van der Straten, "Cooling and trapping of neutral atoms," Phys. Reports **244**, 203–286 (1994).
11. T. Lévèque, L. Antoni-Micollier, B. Faure, and J. Berthon, "A laser setup for rubidium cooling dedicated to space applications," Appl. Phys. B **116**, 997–1004 (2014).
12. S. S. Sané, S. Bennetts, J. E. Debs, C. C. N. Kuhn, G. D. McDonald, P. A. Altin, J. D. Close, and N. P. Robins, "11 w narrow linewidth laser source at 780nm for laser cooling and manipulation of rubidium," Opt. Express **20**, 8915 (2012).
13. J. Dong, X. Zeng, S. Cui, J. Zhou, and Y. Feng, "More than 20 w fiber-based continuous-wave single frequency laser at 780 nm," Opt. Express **27**, 35362 (2019).
14. A. Rao, K. Abdelsalam, T. Sjaardema, A. Honardoost, G. F. Camacho-Gonzalez, and S. Fathpour, "Actively-monitored periodic-poling in thin-film lithium niobate photonic waveguides with ultrahigh nonlinear conversion efficiency of 4600 %w-1cm-2," Opt. Express **27**, 25920 (2019).
15. T. Umeki, O. Tadanaga, and M. Asobe, "Highly efficient wavelength converter using direct-bonded PPZnLN ridge waveguide," IEEE J. Quantum Electron. **46**, 1206–1213 (2010).
16. C. Wang, C. Langrock, A. Marandi, M. Jankowski, M. Zhang, B. Desiatov, M. M. Fejer, and M. Lončar, "Ultrahigh-efficiency wavelength conversion in nanophotonic periodically poled lithium niobate waveguides," Optica **5**, 1438 (2018).
17. J. Lu, J. B. Surya, X. Liu, A. W. Bruch, Z. Gong, Y. Xu, and H. X. Tang, "Periodically poled thin-film lithium niobate microring resonators with a second-harmonic generation efficiency of 250,000%/w," Optica **6**, 1455 (2019).

18. L. Ming, C. B. E. Gawith, K. Gallo, M. V. O'Connor, G. D. Emmerson, and P. G. R. Smith, "High conversion efficiency single-pass second harmonic generation in a zinc-diffused periodically poled lithium niobate waveguide," Opt. Express **13**, 4862 (2005).

19. K. R. Parameswaran, R. K. Route, J. R. Kurz, R. V. Roussev, M. M. Fejer, and M. Fujimura, "Highly efficient second-harmonic generation in buried waveguides formed by annealed and reverse proton exchange in periodically poled lithium niobate," Opt. Lett. **27**, 179 (2002).

20. S. Pal, B. K. Das, and W. Sohler, "Photorefractive damage resistance in ti:PPLN waveguides with ridge geometry," Appl. Phys. B **120**, 737–749 (2015).

21. S. Kurimura, Y. Kato, M. Maruyama, Y. Usui, and H. Nakajima, "Quasi-phase-matched adhered ridge waveguide in LiNbO3," Appl. Phys. Lett. **89**, 191123 (2006).

22. S. A. Berry, L. G. Carpenter, A. C. Gray, P. G. R. Smith, and C. B. E. Gawith, "Zn-indiffused diced ridge waveguides in MgO:PPLN generating 1 watt 780 nm SHG at 70% efficiency," OSA Continuum **2**, 3456 (2019).

23. L. Wang, C. E. Haunhorst, M. F. Volk, F. Chen, and D. Kip, "Quasi-phase-matched frequency conversion in ridge waveguides fabricated by ion implantation and diamond dicing of MgO:LiNbO_3 crystals," Opt. Express **23**, 30188 (2015).

24. H. Hu, R. Ricken, W. Sohler, and R. B. Wehrspohn, "Lithium niobate ridge waveguides fabricated by wet etching," IEEE Photonics Technol. Lett. **19**, 417–419 (2007).

25. V. Boutou, A. Vernay, C. Félix, F. Bassignot, M. Chauvet, D. Lupinski, and B. Boulanger, "Phase-matched second-harmonic generation in a flux grown ktp crystal ridge optical waveguide," Opt. Lett. **43**, 3770–3773 (2018).

26. N. Kretzschmar, U. Eismann, F. Sievers, F. Chevy, and C. Salomon, "2.4-watts second-harmonic generation in ppzno:ln ridge waveguide for lithium laser cooling," Opt. Express **25**, 14840–14855 (2017).

27. R. Bege, D. Jedrzejczyk, G. Blume, J. Hofmann, D. Feise, K. Paschke, and G. Trankle, "Watt-level second-harmonic generation at 589nm with a ppmgo:ln ridge waveguide crystal pumped by a dbr tapered diode laser," Opt. Lett. **41**, 1530–1535 (2016).

28. M. Chauvet, F. Henrot, F. Bassignot, F. Devaux, L. Gauthier-Manuel, V. Pêcheur, H. Maillotte, and B. Dahmani, "High efficiency frequency doubling in fully diced LiNbO3 ridge waveguides on silicon," J. Opt. **18**, 085503 (2016).

29. D. E. Zelmon, D. L. Small, and D. Jundt, "Infrared corrected sellmeier coefficients for congruently grown lithium niobate and 5 mol% magnesium oxide –doped lithium niobate," J. Opt. Soc. Am. B **14**, 3319 (1997).

30. F. Bassignot, E. Courjon, G. Ulliac, S. Ballandras, J.-M. Lesage, and R. Petit, "Acoustic resonator based on periodically poled transducers: Fabrication and characterization," J. Appl. Phys. **112**, 074108 (2012).

31. A. C. Gray, S. A. Berry, L. G. Carpenter, J. C. Gates, P. G. R. Smith, and C. B. E. Gawith, "Investigation of PPLN waveguide uniformity via second harmonic generation spectra," IEEE Photonics Technol. Lett. **32**, 63–66 (2020).

32. R. W. Boyd, *Nonlinear Optics* (Elsevier, 2003).

33. P. Yeh and W. E. Moerner, "Introduction to photorefractive nonlinear optics," Phys. Today **47**, 45–46 (1994).

34. Y. Furukawa, K. Kitamura, S. Takekawa, A. Miyamoto, M. Terao, and N. Suda, "Photorefraction in LiNbO3 as a function of [li]/[nb] and MgO concentrations," Appl. Phys. Lett. **77**, 2494–2496 (2000).

35. B. Chen, J. F. Campos, W. Liang, Y. Wang, and C.-Q. Xu, "Wavelength and temperature dependence of photorefractive effect in quasi-phase-matched LiNbO3 waveguides," Appl. Phys. Lett. **89**, 043510 (2006).

36. L. G. Carpenter, S. A. Berry, A. C. Gray, J. C. Gates, P. G. R. Smith, and C. B. E. Gawith, "CW demonstration of SHG spectral narrowing in a PPLN waveguide generating 2.5 w at 780 nm," Opt. Express **28**, 21382 (2020).